Chemical Science

ROYAL SOCIETY OF CHEMISTRY

EDGE ARTICLE

View Article Online
View Journal | View Issue

Check for updates

Cite this: *Chem. Sci.*, 2022, **13**, 4902

All publication charges for this article have been paid for by the Royal Society of Chemistry

Open Access Article. Published on 01 April 2022. Downloaded on 6/20/2026 6:54:21 AM. This article is licensed under a Creative Commons Attribution 3.0 Unported Licence.

An electrically conductive metallocycle: densely packed molecular hexagons with π-stacked radicals†

Mengxing Cui,[a] Ryuichi Murase,[a] Yongbing Shen,[a] Tetsu Sato,[a] Shohei Koyama,[a] Kaiji Uchida,[a] Tappei Tanabe,[a] Shinya Takaishi,[a] Masahiro Yamashita[ab] and Hiroaki Iguchi ‡*[a]

Electrical conduction among metallocycles has been unexplored because of the difficulty in creating electronic transport pathways. In this work, we present an electrocrystallization strategy for synthesizing an intrinsically electron-conductive metallocycle, $[Ni_6(NDI\text{-}Hpz)_6(dma)_{12}(NO_3)_6]\cdot 5DMA\cdot nH_2O$ (**PMC-hexagon**) (NDI-Hpz = *N*,*N*′-di(1*H*-pyrazol-4-yl)-1,4,5,8-naphthalenetetracarboxdiimide). The hexagonal metallocycle units are assembled into a densely packed ABCABC… sequence (like the fcc geometry) to construct one-dimensional (1D) helical π-stacked columns and 1D pore channels, which were maintained under the liberation of H_2O molecules. The NDI cores were partially reduced to form radicals as charge carriers, resulting in a room-temperature conductivity of (1.2–2.1) × 10^{-4} S cm^{-1} (pressed pellet), which is superior to that of most NDI-based conductors including metal–organic frameworks and organic crystals. These findings open up the use of metallocycles as building blocks for fabricating conductive porous molecular materials.

Received 22nd January 2022
Accepted 23rd March 2022

DOI: 10.1039/d2sc00447j

rsc.li/chemical-science

Introduction

Giant macrocycles have attracted a great deal of attention due to their distinctive molecular structures and diverse functions.[1] Coordination-driven self-assembly is a simple but powerful approach towards synthesizing giant metal–organic macrocycles (so-called metallocycles).[2] Given the high designability of organic linkers and their various combinations with metal ions, metallocycles have provided a wide variety of molecular architectures such as rings,[3,4] polygons,[5–8] polyhedra,[7–9] and nanotubes,[10–14] in tandem with their multifunctional nature. For instance, anticancer ability,[15] drug delivery,[16] chirality recognition,[17] and other molecular responsive functions[3,11,18] have been realized by the flexible cavity of metallocycles. Furthermore, organic linkers with unique electronic properties have been key to fabricating functional metallocycles such as luminescent liquid crystals,[19] asymmetric catalysts,[20] and artificial light-harvesting systems.[21] Although some metallocycles are not isolable in solution, solid-state functions have also been a subject of active research recently. To date, single-molecule magnet behavior,[10,22] solid-state luminescence,[23] heterogeneous catalytic behavior,[24] gas storage,[25] *etc.*, have been reported in crystalline metallocycle assemblies. In this context, engendering electron transfer between assembled metallocycles is promising for providing conductivity as a new function of metallocycles, and moreover, it can be an alternative approach to design conductive porous crystals such as metal–organic frameworks (MOFs).[26] However, only the hole mobility of dipyrrin-based polygons has been reported as the charge-transport property in metallocycles.[27] Intrinsic conductivity, which requires both rich charge carriers and through-space conduction pathways among metallocycles, has not been realized thus far.

Electrocrystallization is a reasonable method to fulfill the above requirements, because the unpaired electrons (π-radicals) generated on π-conjugated planes by a redox reaction can be charge carriers and also induce an attractive interaction between π-conjugated planes. It has been widely used for the syntheses of organic conductors[28] and, more recently, porous molecular conductors (PMCs),[29,30] which are porous crystals consisting of linear coordination polymers with a conductive π-stacked array of *N*,*N*′-di(4-pyridyl)-1,4,5,8-naphthalenetetracarboxdiimide (NDI-py) linkers. The NDI core is a well-known electron acceptor used in various research fields[31] such as self-

[a]*Department of Chemistry, Graduate School of Science, Tohoku University, 6-3 Aza-Aoba, Aramaki, Sendai 980-8578, Japan. E-mail: h-iguchi@tohoku.ac.jp*

[b]*School of Materials Science and Engineering, Nankai University, Tianjin 300350, P. R. China*

† Electronic supplementary information (ESI) available: general information, characterization, crystallographic parameters, magnetism, electrical conductivity and computational method. CCDC 2091485 (**PMC-hexagon**). CCDC 2091485. For ESI and crystallographic data in CIF or other electronic format see DOI: 10.1039/d2sc00447j

‡ Present address: Department of Materials Chemistry, Graduate school of Engineering, Nagoya University, Furo-cho, Chikusa-ku, Nagoya 464-8603, Japan. E-mail: hiroaki.iguchi@chembio.nagoya-u.ac.jp

© 2022 The Author(s). Published by the Royal Society of Chemistry

Open Access Article. Published on 01 April 2022. Downloaded on 6/20/2026 6:54:21 AM.
This article is licensed under a Creative Commons Attribution 3.0 Unported Licence.

assembly,[32] molecule sensors[33] and molecular electronics,[34] whereas its application in intrinsic electron conductors is still in the early stage of development.

Herein, we report an electrically conductive metallocycle synthesized by electrocrystallization for the first time. The coordination-driven self-assembly of hexagonal metallocycle units and the columnar self-assembly of π-conjugated organic linkers occurred together in the electrocrystallization process. In this work, pyrazole was selected as the terminal group of the organic linker because of their preferential construction of various bent coordination polymers[35] and metallocycles.[36]

Results and discussion

Synthesis and discrete metallocycle structure

N,*N*′-Di(1*H*-pyrazol-4-yl)-1,4,5,8-naphthalenetetracarboxdiimide (NDI-Hpz) and $Ni(NO_3)_2 \cdot 6H_2O$ were dissolved in *N*,*N*-dimethylacetamide (DMA) with a small portion of H_2O. Electrocrystallization was carried out by applying a constant direct current of 20 μA to the mixed solution at room temperature (RT). Needle-like tiny black crystals of $[Ni_6(NDI\text{-}Hpz)_6(dma)_{12}(NO_3)_6] \cdot 5DMA \cdot nH_2O$ (hereafter abbreviated as **PMC-hexagon**) were obtained from the cathode in 12 hours.

Single-crystal X-ray diffraction (SXRD) analysis revealed that **PMC-hexagon** crystallized in the trigonal space group $R\bar{3}$ (Table S1†) with merohedral twinning. Remarkably, the hexagonal metallocycle structure $[Ni_6(NDI\text{-}Hpz)_6(dma)_{12}(NO_3)_6]$ constructed from head-to-tail connection between Ni^{2+} ions and NDI-Hpz linkers was elucidated as shown in Fig. 1a and b. A Ni^{2+} ion is coordinated by two pyrazole groups, two DMA molecules in cis geometry, and a bidentate NO_3^- ion. As a result, the Ni^{2+} ion forms nearly octahedral coordination geometry (Fig. 1c). The positions of Ni^{2+} centres and the centroids of NDI cores deviate from the mean plane of the hexagon (1.967 Å and 0.402 Å, respectively), resulting in a pucker of the 6-membered metallocycle (Fig. 1b). The slightly large coordination-bond angle ($\angle$N–Ni–N = 95.9(3)°) and the flexible dihedral angles between the NDI core and each pyrazole plane (60.39° and 62.79°) enable the puckered hexagon structure. In addition, a non-coordinating DMA molecule is located between two pyrazole groups with N–H···O(=C)···H–N hydrogen bonds (Fig. 1c). Since its occupancy is 84%, the total number of hydrogen-bonded DMA molecules is calculated to be five per metallocycle, in accord with the integration ratio in the ^1H NMR spectrum (Fig. S7, ESI†).

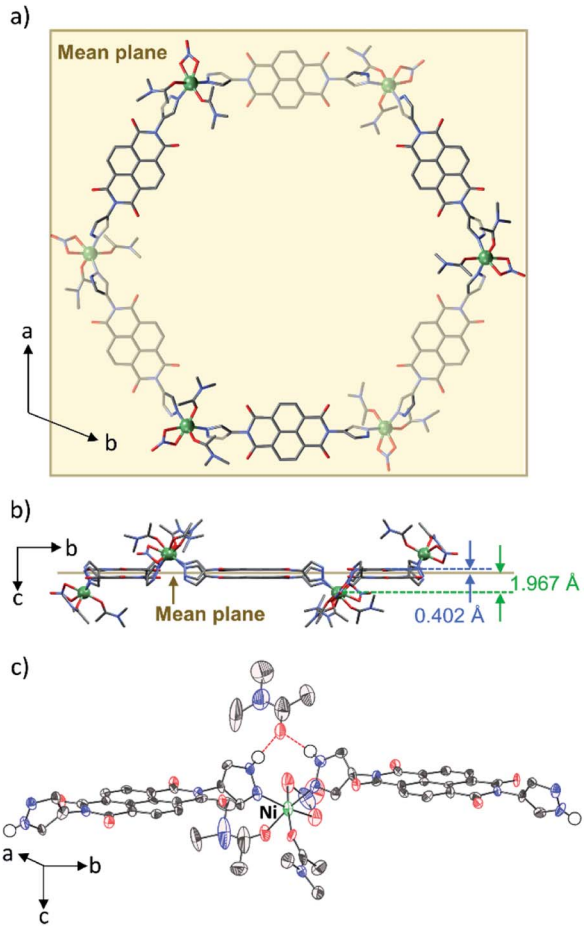

Fig. 1 (a) Crystal structure of the hexagonal metallocycle in **PMC-hexagon**. The atoms under the mean plane of the hexagon are shaded. (b) Perspective view of the hexagonal metallocycle along the *a* axis showing the deviation of Ni^{2+} ions and the centroids of NDI cores from the mean plane of the hexagon. (c) Thermal ellipsoid plot of the ligands around Ni^{2+} ions including hydrogen-bonded DMA. Hydrogen bonds between the H atom of the pyrazole groups and the DMA are represented as red dashed lines. Other H atoms are omitted for clarity. Ni green, O red, N blue, and C black.

Packing structure of the metallocycle

These discrete hexagonal metallocycles stack atop one another at the NDI cores. The crystal packing structure of **PMC-hexagon** (Fig. 2a) displays the hexagonal arrangement of the one-dimensional (1D) helical π-stacked columns and 1D pore channels extended along the crystallographic *c* axis. It is constructed from the dense packing of hexagonal metallocycles with an alternating sequence of ABCABC… (Fig. 2b). This stacking manner, which is similar to the face-centered cubic (fcc) geometry, has rarely been observed in the self-assembly of metallocycles.[37] The helical stacking mode of NDI cores in 60° increments (Fig. 2c) plays a crucial role in overlapping the sides of hexagons and forming the ABCABC… sequence. Although the pyrazole group can form a variety of metallocycle-based polygons,[36] hexagons were selectively crystallized probably because of their compatibility with the helical stacking mode mentioned above.

The interplanar distance between adjacent NDI-Hpz ligands along the stacking axis is 3.173 Å (1/3 of the unit cell length c), which is shorter than those (>3.3 Å) between typical neutral NDI cores,[32a,38] indicating the attractive interaction derived from NDI radicals ($NDI^{\bullet -}$) (Fig. 2d).[29,30] The transfer integral between the adjacent LUMO of NDI-Hpz linkers along the stacking axis was calculated to be 315 meV. It is significantly larger than those of neutral NDI-based organic semiconductors (typically less than 100 meV),[39] reflecting the strong π-stacking interaction in **PMC-hexagon**.

© 2022 The Author(s). Published by the Royal Society of Chemistry

Open Access Article. Published on 01 April 2022. Downloaded on 6/20/2026 6:54:21 AM.
This article is licensed under a Creative Commons Attribution 3.0 Unported Licence.

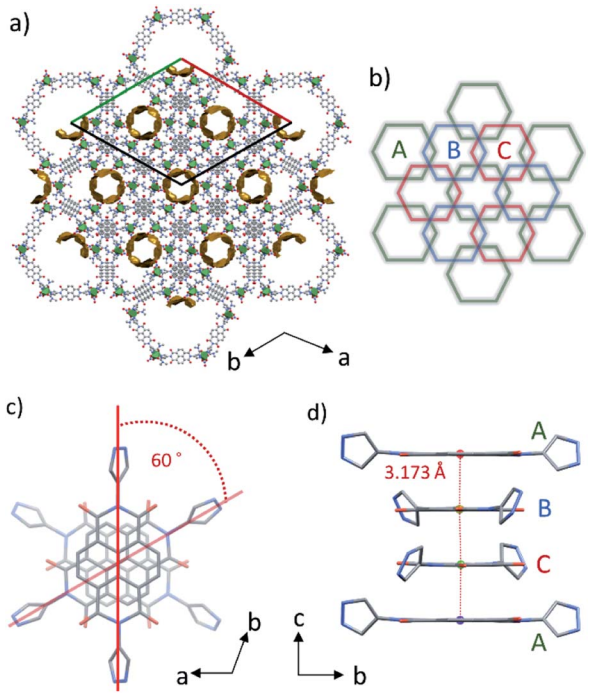

Fig. 2 (a) Crystal packing structure along the *c* axis for **PMC-hexagon**. Coordination sphere around the Ni ion is represented as a green octahedron. The 1D voids of approximately 14.2% of the unit cell volume are mapped by the contact surface (yellow) of a probe with a radius of 1.4 Å. (b) Schematic illustration of the packing mode of hexagons densely stacked with the ABC… sequence. (c) Helical π-stacked column of NDI-Hpz projected along the *c* axis. (d) Side view of the 1D π-stacked column with the interplanar distance.

The dense packing decreases their cavities, resulting in a small void space (14.2% of the total volume). On the basis of elemental analysis, the 1D pore channel is likely to accommodate H_2O molecules (see the Experimental section), whereas their exact number was uncertain because the liberation of H_2O molecules occurred even at RT (Fig. S1, ESI†). After heating **PMC-hexagon** at 120 °C for an hour, the powder X-ray diffraction (PXRD) pattern (Fig. 3) and the number of contained DMA molecules estimated from the integration ratio in the ^{1}H NMR spectrum (Fig. S8, ESI†) were almost unchanged, though a weight loss was observed in thermogravimetry analysis (TGA). These results suggest that the crystal structure was maintained under the liberation of H_2O molecules in the 1D pore channel. The heating of **PMC-hexagon** at 165 °C for an hour induced the liberation of DMA molecules and the deterioration, as suggested by the change of the ^{1}H NMR spectrum (Fig. S9, ESI†) and the PXRD pattern (Fig. 3). Thus, it is difficult to obtain a desolvated state without deterioration in contrast to previously reported PMC with a similar π-stacked analog $[Cd(NDI\text{-}py)(OH_2)_4](NO_3)_{1.3\pm0.1}\cdot n$DMA (PMC-1).[29] However, it is notable that **PMC-hexagon** retained the crystal structure under the liberation of H_2O molecules despite the lack of a coordination polymer network like MOFs. This robustness should originate from the dense packing supported by the strong π-stacking interaction.

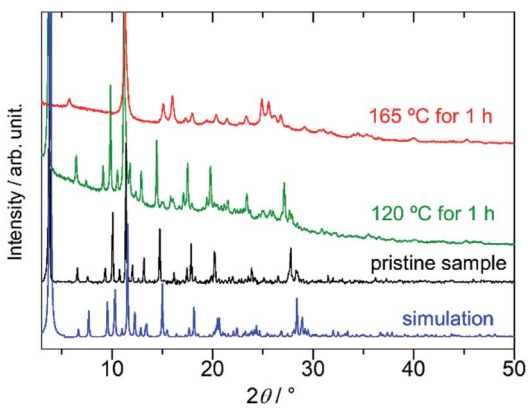

Fig. 3 Powder X-ray diffraction (PXRD) patterns of **PMC-hexagon** (simulated from the crystal structure: blue, pristine sample: black, heated at 120 °C for an hour: green, and heated at 165 °C for an hour: red).

Although the void volume of an individual 1D pore channel is comparable between **PMC-hexagon** and PMC-1 (approx. 820 Å^3 par channel in the unit cell), **PMC-hexagon** was more air-sensitive than PMC-1, probably because the fast liberation of H_2O molecules from the channel promotes the access of oxygen molecules to $NDI^{\bullet-}$ species. The nitrogen gas adsorption in the micropore of **PMC-hexagon** has not been observed (Fig. S10, ESI†), presumably because of the high-vacuum conditions in the activation process. The partial deterioration due to the liberation of DMA molecules probably occurred at least on the surface of the solid during the vacuuming and disturbed the insertion of nitrogen molecules into channels, as suggested by the PXRD pattern (Fig. S11, ESI†) and the ^{1}H NMR spectrum (Fig. S12, ESI†).

Physical properties of PMC-hexagon

The existence of $NDI^{\bullet-}$ was confirmed by a sharp signal (g = 2.00354) in the electron spin resonance (ESR) spectrum (Fig. S2, ESI†). The contribution of $NDI^{\bullet-}$ species to the magnetic properties of **PMC-hexagon** is very small, because the Ni^{2+} ion has a larger spin magnetic moment (S = 1) and the antiferromagnetic interaction and/or partial dimerization along the π-stacked column decreases the total magnetic moment of $NDI^{\bullet-}$ species. We estimated the number of effective $NDI^{\bullet-}$ species in the range from 10 to 15% by fitting the temperature dependence of the $\chi_M T$ value (χ_M: molar spin susceptibility and T: temperature) with the aid of quantum calculations (see Fig. S3† and explanation in the ESI†).

To investigate the electronic state in detail, the solid-state absorption spectra of **PMC-hexagon** and NDI-Hpz dispersed in KBr pellets were acquired. The whole process from the synthesis to the measurement was carried out under an argon atmosphere in order to avoid the air oxidation of radicals. Both spectra display strong absorption bands around 3.3 eV, which are assignable to intramolecular π–π* transition in neutral NDI (NDI^0) cores (Fig. 4).[29,30,40] Additional absorption bands were observed in the spectrum of **PMC-hexagon** as well as reported $NDI^{\bullet-}$ species. The strong band in the range of 2.5–2.8 eV and

© 2022 The Author(s). Published by the Royal Society of Chemistry

Open Access Article. Published on 01 April 2022. Downloaded on 6/20/2026 6:54:21 AM.
This article is licensed under a Creative Commons Attribution 3.0 Unported Licence.

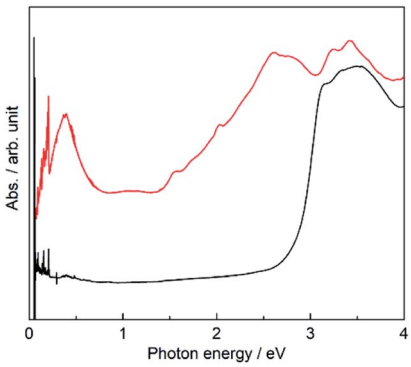

Fig. 4 Solid-state absorption spectra of **PMC-hexagon** (red) and neutral NDI-Hpz (black) dispersed in KBr pellets.

weak bands around 2.0 eV and 1.5 eV are ascribed to the intramolecular electron transition of $NDI^{\bullet-}$.[29,41,42] The weak broad band around 1 eV and the relatively strong band around 0.4 eV are ascribed to the charge transfer (CT) between two $NDI^{\bullet-}$ cores and that from $NDI^{\bullet-}$ to NDI^{0} cores, respectively.[29,30,40,43] The existence of NDI^{0} species in **PMC-hexagon** is inconsistent with the formula, which indicates that the charge of NDI-Hpz is −1. Whilst the concentration of NDI^{0} in the crystal could not be determined with accessible analytical methods, we believe that partial deprotonation of the Hpz group satisfies charge neutrality in this system. The partial absence of the hydrogen-bonded DMA molecules (84% occupancy) may reflect the loss of hydrogen donors due to the partial deprotonation.

The low energy CT band suggests that **PMC-hexagon** is a narrow-gap semiconductor. Since the single crystals of **PMC-hexagon** were too small to measure the electrical conductivity (σ), the measurements were carried out on 3 mmϕ pressed pellets. The current–voltage (I–V) plots indicate the ohmic characteristic ($V = RI$, where R is the electrical resistance) as shown in Fig. 5a. The σ of **PMC-hexagon** at RT was calculated to be $(1.2–2.1) \times 10^{-4}$ S cm^{-1}. It is 10 times higher than the σ of PMC-1, which was newly prepared and measured under the same inert conditions in this work (Fig. S4, ESI†). Note that the σ of PMC-1 in previous work ($(1.5–7.6) \times 10^{-6}$ S cm^{-1})[29] was obtained under incompletely inert conditions and is lower than that obtained in the present work ($(1.4–2.0) \times 10^{-5}$ S cm^{-1} in pressed pellets), indicating that the avoidance of air oxidation is important to properly measure σ in NDI-based conductors. The π-stacked columns in **PMC-hexagon** are surrounded by Ni complexes and are away from 1D pore channels, freeing it from the perturbation of conduction carriers by disordered molecules in the pores. It may be one of the reasons for the 10-fold increase in conductivity compared to PMC-1. The temperature dependence of σ (Fig. 5b) shows the decrease in σ with decreasing temperature, namely semiconducting behavior. The activation energy (E_a) is determined to be 0.148 eV by fitting the data with the Arrhenius equation $\sigma = \sigma_0 \exp(-E_a/kT)$, where σ_0 is the prefactor, k is the Boltzmann constant and T is the temperature. The E_a of **PMC-hexagon** is smaller than that in PMC-1 (0.25 eV),[29] supporting the highly conducting nature of

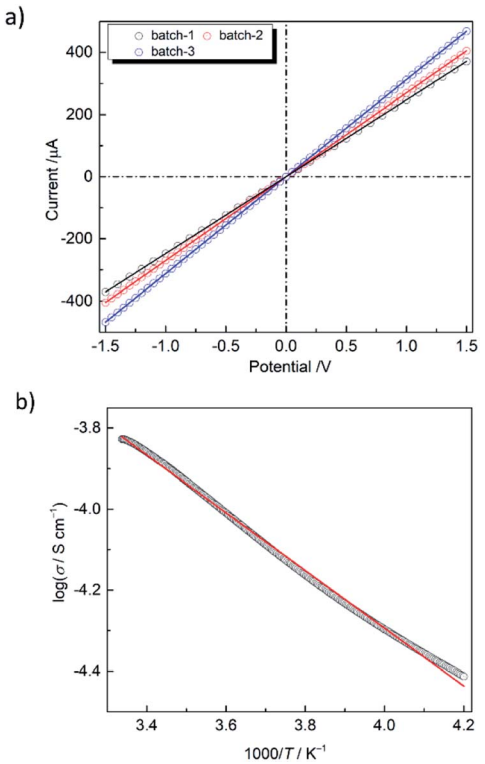

Fig. 5 (a) Current–voltage (I–V) characteristics of **PMC-hexagon** in three different pellets at RT. (b) Temperature dependence of the electrical conductivity (σ) of **PMC-hexagon** fitted with the Arrhenius equation (red line).

PMC-hexagon. To date, the reported σ of NDI-based conductive MOFs/coordination polymers[29,44] and organic crystals[45] have been in the range from 10^{-7} to 2.0×10^{-5} S cm^{-1} for pressed pellets and up to 3.3×10^{-3} S cm^{-1} for single crystals. The σ of a pressed pellet of 1D conductors is typically smaller than that of the single crystal by two to three orders of magnitude. Therefore, **PMC-hexagon** is one of the most conductive NDI-based crystals. Although the σ of **PMC-hexagon** is lower than the record values for conductive MOFs with through-space conduction pathways (10^{-4} to 0.05 S cm^{-1} for lanthanide-hexahydroxytriphenylene-based MOFs),[46] it is higher than that of other π-stacked MOFs (*e.g.* 10^{-9} to 7.6×10^{-5} S cm^{-1} (pressed pellet) for MOFs with a TTF moiety[47]). Moreover, the high σ (above 0.1 S cm^{-1}) observed in some NDI-based polymers[48] implies that we have much room to improve the conductivity of NDI-based metallocycles, which can be an alternative building block to construct conductive porous molecular crystals.

Conclusions

Intrinsically electron-conductive metallocycle **PMC-hexagon** was synthesized by using electrocrystallization. The hexagonal metallocycles were densely π-stacked in a face-centered cubic (fcc)-like geometry (ABCABC… sequence) to afford 1D helical π-stacked conductive columns and 1D pore channels. The radical

Open Access Article. Published on 01 April 2022. Downloaded on 6/20/2026 6:54:21 AM. This article is licensed under a Creative Commons Attribution 3.0 Unported Licence.

at the NDI core ($NDI^{\bullet-}$) provides quite a short interplanar distance (3.173 Å) and conducting carriers, resulting in a high electrical conductivity ($(1.2–2.1) \times 10^{-4}$ S cm^{-1} at RT) even in the polycrystalline pellet sample. Despite the lack of a coordination polymer network, the dense packing of hexagonal metallocycles provides a robust structure, which was maintained under the liberation of H_2O molecules in the pore channels. The elimination of DMA molecules induced the deterioration and disturbed the nitrogen adsorption to pore channels. Although the improvement of the robustness and the conductivity remains to be addressed, the concept of using a metallocycle as a building block provides a new platform for developing electrically conductive porous molecular materials.

Experimental

Materials and characterization

All purchased chemicals were used without further purification. ^{1}H NMR spectra were recorded on a Bruker AVANCE 500 spectrometer at RT. ^{1}H NMR chemical shifts were referenced internally to residual solvent resonances. Deuterated solvents were obtained from Wako and used as received. Electrocrystallization was performed using a direct current (DC) multisource, YAZAWA CS-12Z, and 0.3 mm electrodes of platinum-iridium alloy wires (Pt : Ir = 80 : 20). All elemental analyses were performed at a J-SCIENCE LAB, JM-11 at the Research and Analytical Centre, Tohoku University. Japan.

Synthetic procedures

Synthesis of 4-nitropyrazole. Pyrazole (2.05 g, 29.6 mmol) was dissolved in H_2SO_4 (98%) (6 mL) and cooled to 0 °C. HNO_3 (*ca.* 67%) (1.2 mL) was then added dropwise over 5 minutes. The mixture was then heated to 60 °C and stirred for 2 hours. The mixture was then cooled to 0 °C, the acidic solution was poured into *ca.* 100 g of ice and then stirred for 10 minutes upon which, a white precipitate was formed. The mixture was neutralized with $Na_2CO_{3(aq)}$, extracted with ethyl acetate (100 mL × 3), washed with brine solution, and concentrated to yield a white crystalline powder. The product was recrystallized from ethyl acetate and dried *in vacuo*. Yield: 2.059 g (61.2%). ^{1}H NMR (DMSO-d_6, 500 MHz): δ 13.94 (s, 1H), 8.87 (s, 1H), 8.25 (s, 1H) ppm. Elemental analysis, found: C, 31.95; H, 2.7; N, 37.2. Calc. for $C_3H_3N_3O_2$: C, 31.85; H, 2.7; N, 37.2.

Synthesis of 4-aminopyrazole. 4-Nitropyrazole (2.867 g, 25.4 mmol) was dissolved in anhydrous EtOH (100 mL) in a Schlenk flask and degassed under N_2 for 1 hour. Pd/C powder (10% w/w) was then added and the mixture was further degassed for 1 hour. The flask was then put under reduced pressure and a H_2 gas-filled balloon (1 atm) was then connected. The reaction mixture was then stirred vigorously for 24 hours. The H_2 gas was refilled upon depletion during the reaction. Upon completion of the reaction, the Pd/C powder was separated *via* filtration, and the volume of the filtrate was reduced to yield a reddish oil which partially solidified upon cooling to 5 °C overnight. The product is hygroscopic in ambient air. Yield: 2.04 g (95.5%). ^{1}H NMR (D_2O, 500 MHz): δ 7.28 (s, 2H) ppm. Elemental analysis, found: C, 42.1; H, 6.1; N, 48.7. Calc. for $C_3H_5N_3$: C, 43.35; H, 6.1; N, 50.6. (Note: discrepancy is due to the hygroscopic nature of the product).

Synthesis of *N*,*N*′-di(1*H*-pyrazol-4-yl)-1,4,5,8-naphthalenetetra-carboxdiimide (NDI-Hpz). 4-Aminopyrazole (654 mg, 7.78 mmol) and 1,4,5,8-naphthalenetetracarboxylic dianhydride (1.011 g, 3.97 mmol) were suspended in DMF (40 mL) and degassed for 20 minutes. The reaction was put under N_2 and refluxed for 24 hours. Upon cooling to RT, 80 mL of H_2O was added to the mixture while stirring to yield a yellow/maroon precipitate. The precipitate was filtered, washed with acetone (30 mL × 3), and dried under air. The product was recrystallized from *N*,*N*-dimethylacetamide (DMA) and H_2O to yield a light-yellow powder. Single crystals of NDI-Hpz were obtained by slow diffusion of MeOH to a saturated NDI-Hpz solution in DMA. Yield: 1.35 g (43.6%). ^{1}H NMR (DMSO-d_6, 500 MHz; see Fig. S5, ESI†): δ 13.10 (s, 2H), 8.71 (s, 4H), 7.95 (s, 2H), 7.63 (s, 2H) ppm. Elemental analysis, found: C, 60.15; H, 2.7; N, 21.0. Calc. for $C_{20}H_{10}N_6O_4$: C, 60.3; H, 2.5; N, 21.1.

Synthesis of $[Ni_6(NDI\text{-}Hpz)_6(dma)_{12}(NO_3)_6]\cdot 5DMA\cdot nH_2O$ (PMC-hexagon). For the synthesis of bulk **PMC-hexagon**, NDI-Hpz (20 mg, 0.050 mmol) was suspended in DMA (6 mL) and heated until all solids were dissolved. Upon cooling to RT, the solution was degassed under N_2 for about 30 minutes. To the solution, $Ni(NO_3)_2\cdot 6H_2O$ (29.1 mg, 0.100 mmol) and H_2O (20 μL) were added and sonicated for around 3 minutes. The solution was then put under a constant current of 20 μA. A black microcrystalline product began to appear around the cathode overnight. After the reaction was continued for about 3 days, the product was carefully removed from the cathode and washed with degassed DMA solution under an N_2 atmosphere and dried in glovebox filled with an Ar atmosphere. To obtain single crystals suitable for structural analysis, a degassed DMA solution (3 mL) containing NDI-Hpz (2.6 mg, 6.5 μmol), $Ni(NO_3)_2\cdot 6H_2O$ (3.8 mg, 13 μmol) and H_2O (20 μL) was prepared. After a constant current of 20 μA was applied to the solution overnight, black needle-like crystals of **PMC-hexagon** were obtained. Elemental analysis, found: C, 47.2; H, 4.9; N, 16.8. Calcd for $C_{188}H_{237}N_{59}Ni_6O_{71}$: C, 46.9; H, 5.0; N, 17.2 (assumed that n = 12). (Note: due to the liberation of H_2O molecules at RT, the number of lattice H_2O molecules depends on the elapsed time since the sample filtration).

Data availability

Detailed data including general information, characterization, crystallographic parameters, magnetism, electrical conductivity and computational methods are available in the ESI.†

Author contributions

H. I. conceived and designed the project. M. C. carried out the synthesis, characterization, crystal structure analysis and measuring of the physical properties of **PMC-hexagon**. R. M. contributed to the design of the experiment, syntheses of ligands and **PMC-hexagon**, and preliminary crystal structure analysis. Y. S. contributed to the measurement and analysis of

© 2022 The Author(s). Published by the Royal Society of Chemistry

Open Access Article. Published on 01 April 2022. Downloaded on 6/20/2026 6:54:21 AM. This article is licensed under a Creative Commons Attribution 3.0 Unported Licence.

electrical conductivity. T. S. and K. U contributed to the magnetic measurements and the analyses using calculation and fitting. K. U. also contributed to the nitrogen adsorption measurement. S. K. performed the theoretical calculation of the transfer integral. T. T. contributed to measurements and characterization related to nitrogen sorption isotherms and the thermogravimetry analysis. S. T., M. Y. and H. I. supervised this work and carried out discussions. M. C. and H. I. wrote the paper.

Conflicts of interest

There are no conflicts to declare.

Acknowledgements

We acknowledge the support from Prof Akutagawa and Dr Hoshino at Tohoku University for acquiring the ESR spectra. We also thank Prof Iwamoto and Dr Ishida at Tohoku University for the preliminary SXRD analysis. This work was partly supported by JSPS KAKENHI Grant Numbers JP18H04498 (H. I.), JP19H05631 (H. I., S. T. and M. Y.), JP21H01901 (H. I.) and JP21K18971 (H. I.), by the Toyota Riken Scholar Program (H. I.), by the Kato Foundation for Promotion of Science KJ-2916 (H. I.), and by the Iketani Science and Technology Foundation 0331101-A (H. I.). M. Y. acknowledges the support from the 111 project (B18030) from China. M. C. gratefully acknowledges the financial support from the Chinese Scholarship Council (CSC).

Notes and references

1 (*a*) K. Y. Cheung, Y. Segawa and K. Itami, *Chem.–Eur. J.*, 2020, **26**, 14791–14801; (*b*) D. Xia, P. Wang, X. Ji, N. M. Khashab, J. L. Sessler and F. Huang, *Chem. Rev.*, 2020, **120**, 6070–6123; (*c*) Y. Zhou, K. Jie, R. Zhao and F. Huang, *Adv. Mater.*, 2020, **32**, 1904824.

2 (*a*) M. Fujita, J. Yazaki and K. Ogura, *J. Am. Chem. Soc.*, 1990, **112**, 5645–5647; (*b*) T. R. Cook and P. J. Stang, *Chem. Rev.*, 2015, **115**, 7001–7045; (*c*) W. Wang, Y.-X. Wang and H.-B. Yang, *Chem. Soc. Rev.*, 2016, **45**, 2656–2693.

3 S. Kawano, T. Fukushima and K. Tanaka, *Angew. Chem., Int. Ed.*, 2018, **57**, 14827–14831.

4 R. Miyake, A. Ando, M. Ueno and T. Muraoka, *J. Am. Chem. Soc.*, 2019, **141**, 8675–8679.

5 G.-Y. Wu, L.-J. Chen, L. Xu, X.-L. Zhao and H.-B. Yang, *Coord. Chem. Rev.*, 2018, **369**, 39–75.

6 Y. Sakata, R. Yamamoto, D. Saito, Y. Tamura, K. Maruyama, T. Ogoshi and S. Akine, *Inorg. Chem.*, 2018, **57**, 15500–15506.

7 H. Sepehrpour, W. Fu, Y. Sun and P. J. Stang, *J. Am. Chem. Soc.*, 2019, **141**, 14005–14020.

8 S. Chakraborty and G. R. Newkome, *Chem. Soc. Rev.*, 2018, **47**, 3991–4016.

9 M. Yamashina, Y. Tanaka, R. Lavendomme, T. K. Ronson, M. Pittelkow and J. R. Nitschke, *Nature*, 2019, **574**, 511–515.

10 J. Wu, L. Zhao, L. Zhang, X.-L. Li, M. Guo, A. K. Powell and J. Tang, *Angew. Chem., Int. Ed.*, 2016, **55**, 15574–15578.

11 G. Li, W. Yu and Y. Cui, *J. Am. Chem. Soc.*, 2008, **130**, 4582–4583.

12 L. Zhang, L. Lin, D. Liu, Y.-J. Lin, Z.-H. Li and G.-X. Jin, *J. Am. Chem. Soc.*, 2017, **139**, 1653–1660.

13 Z. Y. Chen, B. Sahli and M. J. MacLachlan, *Inorg. Chem.*, 2017, **56**, 5383–5391.

14 K. Otake, K. Otsubo, T. Komatsu, S. Dekura, J. M. Taylor, R. Ikeda, K. Sugimoto, A. Fujiwara, C.-P. Chou, A. W. Sakti, Y. Nishimura, H. Nakai and H. Kitagawa, *Nat. Commun.*, 2020, **11**, 843.

15 A. A. Adeyemo, A. Shettar, I. A. Bhat, P. Kondaiah and P. S. Mukherjee, *Inorg. Chem.*, 2017, **56**, 608–617.

16 W. Cullen, S. Turega, C. A. Hunter and M. D. Ward, *Chem. Sci.*, 2015, **6**, 625–631.

17 J. Dong, C. Tang, K. Zhang, Y. Liu, P. Low, J. Jiang and Y. Cui, *J. Am. Chem. Soc.*, 2017, **139**, 1557–1564.

18 B. Shi, Z. Zhou, R. T. Vanderlinden, J.-H. Tang, G. Yu, K. Acharyya, H. Sepehrpour and P. J. Stang, *J. Am. Chem. Soc.*, 2019, **141**, 11837–11841.

19 L. Chen, C. Chen, Y. Sun, S. Lu, H. Huo, T. Tan, A. Li, X. Li, G. Ungar, F. Liu and M. Zhang, *Angew. Chem., Int. Ed.*, 2020, **59**, 10143–10150.

20 T. Hong, Z. Zhang, Y. Sun, J.-J. Tao, J.-D. Tang, C. Xie, M. Wang, F. Chen, S.-S. Xie, S. Li and P. J. Stang, *J. Am. Chem. Soc.*, 2020, **142**, 10244–10249.

21 D. Zhang, W. Yu, S. Li, Y. Xia, X. Li, Y. Li and T. Yi, *J. Am. Chem. Soc.*, 2021, **101**, 1313–1317.

22 (*a*) J. Wu, X.-L. Li, M. Guo, L. Zhao, Y.-Q. Zhang and J. Tang, *Chem. Commun.*, 2018, **54**, 1065–1068; (*b*) J. Lu, V. Montigaud, O. Cador, J. Wu, L. Zhao, X.-L. Li, M. Guo, B. Le Guennic and J. Tang, *Inorg. Chem.*, 2019, **58**, 11903–11911.

23 M. El Sayed Moussa, S. Evariste, H.-L. Wong, L. Le Bras, C. Roiland, L. Le Polles, B. Le Guennic, K. Costuas, V. W.-W. Yam and C. Lescop, *Chem. Commun.*, 2016, **52**, 11370–11373.

24 (*a*) S. Tashiro and M. Shionoya, *Acc. Chem. Res.*, 2020, **53**, 632–643; (*b*) P. Rani, A. Sharma, A. Husain, G. Kumar, H. Kaur, K. K. Bhasin and G. Kumar, *CrystEngComm*, 2019, **21**, 7447–7459.

25 (*a*) T. Pietrass, I. Cruz-Campa, J. Kombarakkaran, S. Sirimulla, A. M. Arif and J. C. Noveron, *J. Phys. Chem. C*, 2010, **114**, 21371–21377; (*b*) I. F. Silva, I. F. Teixeira, W. P. Barros, C. B. Pinheiro, J. D. Ardisson, G. M. Do Nascimento, N. A. Pradie, A. P. C. Teixeira and H. O. Stumpf, *J. Mater. Chem. A*, 2019, **7**, 15225–15232.

26 (*a*) L. S. Xie, G. Skorupskii and M. Dincă, *Chem. Rev.*, 2020, **120**, 8536–8858; (*b*) J.-S. M. Lee, K.-I. Otake and S. Kitagawa, *Coord. Chem. Rev.*, 2020, **421**, 213447.

27 H. Maeda, R. Akuta, Y. Bando, K. Takaishi, M. Uchiyama, A. Muranaka, N. Tohnai and S. Seki, *Chem.–Eur. J.*, 2013, **19**, 11676–11685.

28 (*a*) H. Anzai, J. M. Delrieu, S. Takasaki, S. Nakatsuji and J. Yamada, *J. Cryst. Growth*, 1995, **154**, 145–150; (*b*) P. Batail, K. Boubekeur, M. Fourmigué and J.-C. P. Gabriel, *Chem. Mater.*, 1998, **10**, 3005–3015.

Open Access Article. Published on 01 April 2022. Downloaded on 6/20/2026 6:54:21 AM. This article is licensed under a Creative Commons Attribution 3.0 Unported Licence.

29 L. Qu, H. Iguchi, S. Takaishi, F. Habib, C. F. Leong, D. M. D'Alessandro, T. Yoshida, H. Abe, E. Nishibori and M. Yamashita, *J. Am. Chem. Soc.*, 2019, **141**, 6802–6806.

30 S. Koyama, T. Tanabe, S. Takaishi, M. Yamashita and H. Iguchi, *Chem. Commun.*, 2020, **56**, 13109–13112.

31 (*a*) M. Al Kobaisi, S. V. Bhosale, K. Latham, A. M. Raynor and S. V. Bhosale, *Chem. Rev.*, 2016, **116**, 11685–11796; (*b*) S. V. Bhosale, M. Al Kobaisi, R. W. Jadhav, P. P. Morajkar, L. A. Jones and S. George, *Chem. Soc. Rev.*, 2021, **50**, 9845–9998.

32 (*a*) S. K. Keshri, T. Ishizuka, T. Kojima, Y. Matsushita and M. Takeuchi, *J. Am. Chem. Soc.*, 2021, **143**, 3238–3244; (*b*) X. Peng, L. Wang and S. Chen, *J. Inclusion Phenom. Macrocyclic Chem.*, 2021, **99**, 131–154.

33 (*a*) E. Takahashi, H. Takaya and T. Naota, *Chem.–Eur. J.*, 2010, **16**, 4793–4802; (*b*) A. Mallick, B. Garai, M. A. Addicoat, P. S. Petkov, T. Heine and R. Banerjee, *Chem. Sci.*, 2015, **6**, 1420–1425; (*c*) T. Ono, Y. Tsukiyama, S. Hatanaka, Y. Sakatsume, T. Ogoshi and Y. Hisaeda, *J. Mater. Chem. C*, 2019, **31**, 9726–9734; (*d*) T. Tanabe, T. Sato, K. Fuku, K. Uchida, T. Yamauchi, S. Takaishi and H. Iguchi, *Chem. Lett.*, 2021, **50**, 1479–1482.

34 (*a*) H. E. Katz, A. J. Lovinger, J. Johnson, C. Kloc, T. Siegrist, W. Li, Y.-Y. Lin and A. Dodabalapur, *Nature*, 2000, **404**, 478–481; (*b*) K. Takimiya and M. Nakano, *Bull. Chem. Soc. Jpn.*, 2018, **91**, 121–140; (*c*) D. Ohayon, A. Savva, W. Du, B. D. Paulsen, I. Uguz, R. S. Ashraf, J. Rivnay, I. McCulloch and S. Inal, *ACS Appl. Mater. Interfaces*, 2021, **13**, 4253–4266.

35 K. V. Domasevitch, I. Boldog, E. B. Rusanov, J. Hunger, S. Blaurock, M. Schröder and J. Z. Sieler, *Z. Anorg. Allg. Chem.*, 2005, **631**, 1095–1100.

36 (*a*) M. A. Halcrow, *Dalton Trans.*, 2009, **12**, 2059–2073; (*b*) S. Yao, W.-H. Fang, Y. Sun, S.-T. Wang and J. Zhang, *J. Am. Chem. Soc.*, 2021, **143**, 2325–2330.

37 E. Coronado, J. R. Galan-Mascaros, P. Gaviña, C. Martí-Gastaldo, F. M. Romero and S. Tatay, *Inorg. Chem.*, 2008, **47**, 5197–5203.

38 Y. Matsunaga, K. Goto, K. Kubono, K. Sako and T. Shinmyozu, *Chem.–Eur. J.*, 2014, **20**, 7309–7316.

39 (*a*) T. Kakinuma, H. Kojima, M. Ashizawa, H. Matsumoto and T. Mori, *J. Mater. Chem. C*, 2013, **1**, 5395–5401; (*b*) H. Abe, A. Kawasaki, T. Takeda, N. Hoshino, W. Matsuda, S. Seki and T. Akutagawa, *J. Am. Chem. Soc.*, 2021, **143**, 1046–1060.

40 P. M. Usov, C. Fabian and D. M. D'Alessandro, *Chem. Commun.*, 2012, **48**, 3945–3947.

41 C. F. Leong, B. Chan, T. B. Faust and D. M. D'Alessandro, *Chem. Sci.*, 2014, **5**, 4724–4728.

42 D. Gosztola, M. P. Niemczyk, W. Svec, A. S. Lukas and M. R. Wasielewski, *J. Phys. Chem. A*, 2000, **104**, 6545–6551.

43 A. Takai, T. Yasuda, T. Ishizuka, T. Kojima and M. Takeuchi, *Angew. Chem., Int. Ed.*, 2013, **52**, 9167–9171.

44 (*a*) X. Kuang, S. Chen, L. Meng, J. Chen, X. Wu, G. Zhang, G. Zhong, T. Hu, Y. Li and C.-Z. Lu, *Chem. Commun.*, 2019, **55**, 1643–1646; (*b*) H. C. Wentz, G. Skorupskii, A. B. Bonfim, J. L. Mancuso, C. H. Hendon, E. H. Oriel, G. T. Sazama and M. G. Campbell, *Chem. Sci.*, 2020, **11**, 1342–1346; (*c*) K. Fuku, M. Miyata, S. Takaishi, T. Yoshida, M. Yamashita, M. Hoshino, T. Akutagawa, H. Ohtsu, M. Kawano and H. Iguchi, *Chem. Commun.*, 2020, **56**, 8619–8622; (*d*) Y. Yan, S. Henfling, N.-N. Zhang and H. Krautscheid, *Chem. Commun.*, 2021, **57**, 10407–10410.

45 (*a*) G. Heywang, L. Born, H.-G. Fitzky, T. Hassel, J. Hocker, H.-K. Müller, B. Pittel and S. Roth, *Angew. Chem., Int. Ed. Engl.*, 1989, **28**, 483–485; (*b*) A. Mizuno, Y. Shuku, R. Suizu, M. M. Matsushita, M. Tsuchiizu, D. R. Mañeru, F. Illas, V. Robert and K. Awaga, *J. Am. Chem. Soc.*, 2015, **137**, 7612–7615; (*c*) M. T. Nguyen, M. D. Krzyaniak, M. Owczarek, D. P. Ferris, M. R. Wasielewski and J. F. Stoddart, *Angew. Chem., Int. Ed.*, 2017, **56**, 5795–5800.

46 G. Skorupskii, B. A. Trump, T. W. Kasel, C. M. Brown, C. H. Hendon and M. Dincă, *Nat. Chem.*, 2020, **12**, 131–136.

47 (*a*) L. Sun, S. S. Park, D. Sheberla and M. Dincă, *J. Am. Chem. Soc.*, 2016, **138**, 14772–14782; (*b*) H.-Y. Wang, J.-Y. Ge, C. Hua, C.-Q. Jiao, Y. Wu, C. F. Leong, D. M. D'Alessandro, T. Liu and J.-L. Zuo, *Angew. Chem., Int. Ed.*, 2017, **56**, 5465–5470; (*c*) J. Su, T.-H. Hu, R. Murase, H.-Y. Wang, D. M. D'Alessandro, M. Kurmoo and J.-L. Zuo, *Inorg. Chem.*, 2019, **58**, 3698–3706; (*d*) S. Zhang, D. K. Panda, A. Yadav, W. Zhou and S. Saha, *Chem. Sci.*, 2021, **12**, 13379–13391.

48 D. Kiefer, A. Giovannitti, H. Sun, T. Biskup, A. Hofmann, M. Koopmans, C. Cendra, S. Weber, L. J. A. Koster, E. Olsson, J. Rivnay, S. Fabiano, I. McCulloch and C. Müller, *ACS Energy Lett.*, 2018, **3**, 278–285.

© 2022 The Author(s). Published by the Royal Society of Chemistry